ORIGINAL ARTICLE

IWJ WILEY

An injectable metal nanoparticle containing cellulose derivative-based hydrogels: Evaluation of antibacterial and in vitro-vivo wound healing activity in children with burn injuries

Yuming Qiu[1] | Xiuxiang Sun[2] | Xiaoli Lin[3] | Wenying Yi[4] | Jianye Jiang[5]

[1]Department of Ophthalmology, Yantai Yantaishan Hospital, Yantai, China

[2]Department of Respiratory Medicine, Yantai Qishan Hospital, Yantai, China

[3]Department of Acupuncture, massage and rehabilitation, Penglai Traditional Chinese Medicine Hospital, Penglai, China

[4]Department of General Surgery, The Affiliated Yantai Yuhuangding Hospital of Qingdao University, Yantai, China

[5]Department of Pediatrics, Chengyang District People's Hospital of Qingdao, Qingdao, China

Correspondence
Wenying Yi, No. 20 East Yuhuangding Road, Yantai 264000, China.
Email: wenying-yi2@hotmail.com

Jianye Jiang, No. 600 the Great Wall Road, Chengyang 266109, China.
Email: jianye.j@yahoo.com

Abstract

The preparation of hydrogels for wound healing properties with high antibacterial activities and good biosafety concurrently can be relatively challenging. For addressing these issues, we report on the synthesis and characterisation of a nanocomposite hydrogel dressing by introducing the silver nanoparticles in hydroxypropyl methylcellulose-hydroxyapatite scaffold hydrogel (HMC-HA/AgNPs). The different concentrations of AgNPs in HMC-HA/AgNPs hydrogels were confirmed by swelling ratio, degradation, and gelatin time. The synthesised HMC-HA/AgNPs hydrogels were further characterised using the UV-visible, scanning electron microscopy, transmission electron microscopy, Fourier transform infrared spectrum, and X-ray diffraction. The results showed that the novel HMC-HA/AgNPs hydrogel exhibited a porous 3D network and high mechanical properties because of the inter-molecular and intra-molecular interactions. The AgNPs give the HMC-HA hydrogels excellent antibacterial activities against both *Staphylococcus aureus* and *Escherichia coli*, without any chemical reductant and cross-linking agent required endows the hydrogel high biocompatibility. More importantly, HMC-HA/AgNPs effectively repaired wound defects in mice models, and wound healing reached $94.5 \pm 1.4\%$ within 16 days. The HMC-HA hydrogel with AgNPs showed excellent antimicrobial activity and burn wound healing. Therefore, these HMC-HA/AgNPs hydrogels have great potential as an injectable hydrogel for wound healing activity in children with burn injuries.

KEYWORDS

bacterial activity, burn injuries, hydrogels, nanoparticle, wound

Yuming Qiu, Xiuxiang Sun, and Xiaoli Lin contributed equally to this study.

Key Messages
- an injectable HMC-HA/AgNPs composites hydrogel was successfully developed
- the HMC-HA/AgNPs hydrogels have a high swelling and degradation ratio
- HMC-HA/AgNPs exhibited an excellent antibacterial activity
- HMC-HA/AgNPs have an excellent injectable hydrogel for burn wound dressing

1 | INTRODUCTION

With the increasing worldwide prevalence of diabetes, complications such as non-healing, chronic, diabetic wounds have become a serious threat to the health and quality-of-life of patients.[1] Human skin serves as a protective barrier against harsh external conditions, yet it is frequently subjected to conflict, resulting in traumatic wounds that compromise skin's functional integrity.[2] The most extensively used procedures for haemostasis and wound healings are traditional surgical sutures and mechanical fixation. As a result of the fight between bacteria and the immune system, tissue invasion can occur, and infection can result in serious tissue damage. To treat skin damage and trauma, effective and quick wound healing procedures are required. Although numerous therapies for the diagnosis and treatment of chronic wounds are available, their efficacy is usually limited, and relapse occurs in a significant number of patients.[3] The growing number of cases and unsatisfactory treatment outcomes necessitates the development of effective therapeutic approaches. More effective and versatile wound dressings must be created to fulfil the diverse needs of various patients. In recent years, several wound healing treatments have proven to be beneficial, one of which is the use of nanoparticle-controlled chemical delivery systems to transfer antibiotics into the skin tissue.[4]

Metal and metal oxide nanoparticles have been demonstrated to have wide antibacterial properties in research studies.[5] Silver nanocarriers activate antioxidant activity by reducing, donating electrons, and scavenging radicals. As a result, silver nanoparticles (AgNPs) have been identified as a scavenger of reactive oxygen species (ROS) that can reduce the number of free radicals produced during the inflammatory stage of wound healing.[6] AgNPs can be extremely useful in preventing infections in diabetic chronic and non-healing wounds because of their appealing biological activities such as antibacterial, antiviral, antifungal, antioxidant, anti-inflammatory, anti-angiogenesis, and antiplatelet capabilities.[7] Ongoing research on a 3D hydrogel network shows that the large empty space between cross-linked networks in the swelled phase can operate as a nanoreactor for nanoparticle synthesis. The unique nanocomposite systems that come from the in situ synthesis of AgNPs within swelling hydrogel networks have a wide range of applications in biomedical, catalytic, and bioengineering applications. Many researchers have discovered that AgNPs have anti-inflammatory properties, which aid in the speeding up and fine-tuning wound healing.[8] The bactericidal activity of AgNPs is mainly attributed to the Ag^+ produced from them, which can destroy bacteria's critical biomolecules such as cell membranes, DNA, and enzymes.[9] The antibacterial activity of AgNPs has been attributed to Ag^+ ions interacting with bacteria enzymes and proteins, as well as the degradation of the bacteria's membrane.[10] Worse yet, the conditioning coating can exacerbate the inflammatory response of injured tissue, causing tissue damage and obstructing wound healing. To address this issue, surface functionalization of AgNPs with antifouling properties becomes an ideal solution to provide cotton dressings with both bacterial anti-adhesion and bactericidal activities, which will inhibit bacterial adhesion in wound tissue synergistic effect and successfully prevent wound infection.[11]

Because of their highly interconnected porous network, hydrogels offer great features for wet wound healing, such as favourable fluid absorption and excessive water retention.[12] As a result, new natural-synthetic composite hydrogels are being developed, paving the way for customizable porosity architecture, mechanical and physicochemical properties, and exceptional biocompatibility and bioactivity attracted by natural polymers.[13] As the most prevalent natural polymer on the planet, cellulose is inexpensive, biodegradable, and environmentally friendly.[14] Furthermore, cellulose offers several exceptional features, including mechanical durability, water absorption capacity, and biocompatibility, making it an excellent material for wound healing.[15] Hydroxypropyl methylcellulose (HMC) is a type of hydrogel-forming polymer that has a wide range of applications in the industry.[16] HMC can make inter-molecular, intra-molecular, and hydrophobic interactions because of the presence of polar (hydroxypropyl) and non-polar (methyl) groups, depending on the degree of substitution of polar and non-polar groups.[17] The HMC polymer creates a

transparent, colourless hydrogel with high stability, viscosity, and texture modification when exposed to water. This allows HMC to easily merge with other materials for uses like food packaging, wound healing, and medicine delivery.[18] The addition of synthetic hydroxyapatite (HA) to biomaterials improves osseointegration, allowing them to be used for tissue regeneration.[19] The size of HA influences its intrinsic mechanical capabilities as well as its interaction with bone tissues. Recent research on HA-based biomaterials has shown that HA with a nanoscale size favours biological response and demonstrates superior tissue engineering capability.[20] HMC-combined hydrogels have a large number of functional groups, which give enough locations for metal NPs to be stabilised by forming a coordination bond. Green synthesis was used to make HMC-capped AgNPs with a spherical form and sizes ranging from 3 to 17 nm.[21] The produced AgNPs in HMC nanocomposites including bacterial cellulose nanocrystals and AgNPs were also significantly stabilised by the functional groups of HMC and bacterial cellulose nanocrystals.[22]

We report the development of HMC-HA hydrogel-loaded AgNPs for diabetic wound healing. HMC-HA hydrogel-loaded AgNPs were fabricated using reduction of AgNO$_3$ with HMC/HA and was characterised using UV-visible, Fourier transform infrared spectrum (FT-IR), X-ray diffraction (XRD), scanning electron microscopy (SEM), and transmission electron microscopy (TEM), gelation time, equilibrium swelling, and in vitro degradation, as well as tested for its antibacterial properties and wound healing efficacy. The porous structure provided a moist and humid microenvironment that facilitated the absorption of the exudates from the wounded area. Antibacterial and wound healing applications of HMC-HA hydrogel-loaded AgNPs have not been documented so far to our knowledge. As a result, we formed HMC-HA hydrogel-loaded AgNPs dressing materials that are effective antibacterial agents against *Staphylococcus aureus* and *Escherichia coli*, as well as investigating their wound healing performance. This study used effectively in vitro and in vivo research to demonstrate the wound healing effect of AgNPs formulations on rats' skin. As a result, HMC-HA hydrogel-loaded AgNPs could be a potential material for wound healing in children with burn injuries.

2 | MATERIALS AND METHODS

2.1 | Materials

Hydroxypropyl methylcellulose (HPMC), hydroxyapatite (HA), powder, 2.5 μm, ≥100 m^2/g, and AgNO$_3$ were obtained from Sigma-Aldrich and used without further

purification. All other reagents, unless otherwise specified, were of analytical grade and used as received. Throughout the experiment, double distilled water was used.

2.2 | Preparation of HMC-HA hydrogels containing AgNPs

In a typical synthesis, 250 mg of HMC powder was mixed with 50 mL of distilled water to make the mixture. Then, in the already prepared solution, HA was added at a concentration of 0.5% wt/vol. Finally, while stirring, powdered HMC (2% wt/vol) was added. While being agitated, the resultant solution was placed in an ice bath. The completed hydrogel or reinforced hydrogel precursor solutions, which are injectable within the first 10 minutes, are injected into plastic moulds and stored at room temperature in a humid environment. The cross-linking of HMC-HA chains and the attachment of AgNPs to the HMC-HA chains were accomplished in a single step using HMC. To achieve complete dissolution of HMC-HA, 0.5 g of AgNO$_3$ (0.5-2.0 wt%) was added to aqueous solutions containing HMC-HA at 2% wt/vol of HMC and 0.5% wt/vol of HA, and the temperature was raised to 60°C with steady stirring for 1 hour using a magnetic stirrer. The contents were cooled to 15 ± 4°C and centrifuged for 20 minutes at 10000 rpm. During swelling in the AgNO$_3$ solution, the silver ions (Ag$^+$) are stabilised in the hydrogel pores. The metal ions are connected to the functional groups of the HMC-HA hydrogel networks (—NH, —OCH$_3$, —OH, and —COO). Through centrifugation, the collected precipitate was repeatedly rinsed with double distilled water, and the resulting product was kept in a vacuum desiccator until further use.

2.3 | Gelation time

The tube inversion method is used to record the gelation time. The generated AgNPs were evaluated, and after being cleaned, the HMC-HA hydrogel was submerged in distilled water and separated by centrifugation at 5000 rpm for 5 minutes under continuous inversion control. The gelation time was calculated as the time when a polymer solution stopped flowing after 30 seconds of tube inversion.

2.4 | In vitro degradation evaluation of hydrogels

The initial weights of the HMC-HA and HMC-HA/AgNPs hydrogels were measured and labelled W_0. The hydrogels were then submerged in 3.0 mL PBS and agitated

at a speed of 60 rpm/min in a shaker at 37°C. Hydrogels were removed from PBS and the water on the hydrogel surface was wiped off at predetermined time intervals; W_t (day 1, day 3, day 5, day 7, day 10, and day 14). In vitro degradation was calculated using the following equation:

$$\%\text{Degradation}\,(t) = [W_0 - W_t]/W_0$$

2.5 | Swelling experiments

The dynamic swelling features of HMC-HA and HMC-HA/AgNPs hydrogels were investigated in various water solution conditions. Before reaching swelling equilibrium, the weights of HMC-HA and HMC-HA/AgNPs hydrogels were dissolved in PBS and kept at 37°C for 2 hours. The dry hydrogel was then submerged in de-ionised water. The swelling ratio (SR) was computed using the equation given below, where W_0 and W_d are the weight swelling states of the hydrogels and the dry state of the equilibrium, respectively.

$$\text{SR}\,(\%) = (W_0 - W_d)/W_d$$

2.6 | Characterisation

The UV-Vis spectrophotometer (Shimadzu, model UV-1800, Kyoto, Japan) was used to measure the HMC-HA hydrogels solution containing AgNPs in the range of 350 to 650 nm. The surface micrographs of the HMC-HA and HMC-HA/AgNPs hydrogels were studied using a Cressington 108 Auto (Cressington, Watford, United Kingdom) operated at a 10 kV accelerating voltage. To determine the average size of pores on device surfaces, Image J software was used to measure 50 pores (Java 1.8.0). The AgNPs were observed using a transmission electron microscope (TEM, Hitachi HT7700, Tokyo, Japan) operating at 200 kV after hydrating the HMC-HA hydrogels with three volumes of distilled water and soni-cating them for 5 minutes in a bath at a frequency of about 20 kHz on a lacy carbon-coated Cu grid. At ambient circumstances, FT-IR measurements were taken with a Nicolet FT-IR 5700 spectrophotometer (Thermo Fisher Scientific, Waltham, Massachusetts). In a wavelength range of 4000 to 400 cm^{-1}, the HMC-HA, AgNPs, and HMC-HA/AgNPs hydrogel samples were observed. On HMC-HA, AgNPs, and HMC-HA/AgNPs hydrogels, XRD patterns were recorded using a D8 Advance diffractometer (Bruker AXS, Inc., Madison, Wisconsin) with Cu set and K radiation (=0.154 nm) at 30 kV and 40 mA. The scan speed was 2°/min, with a spectral range of 10° to 80°.

2.7 | Antimicrobial activity

The antibacterial activity of the HMC-HA and HMC-HA/AgNPs hydrogels was assessed using the cell count method against Gram-negative bacteria (*E coli*, ATCC 25922) and Gram-positive bacteria (*S aureus*, ATCC 25923). Briefly, 10 μL of bacterial suspension in PBS (10^6 CFU/mL) was uniformly coated on the surface of hydrogels and control, and these samples were incubated at 37°C for 1 hour. To adjust the 2% test sample concentration, the LB medium was separated, the bacteria were washed three times with PBS (pH 7.4), and 1.0 mL of MC/HA and MC-HA/AgNPs hydrogels were applied. Therefore, 5 mL of bacterial dispersion and 5 mL of sterilised culture media were mixed and applied to the hydrogel with and without AgNPs. The plates were then incubated at 37°C for 24 hours with 200 μL of AgNPs solution and formed HMC-HA hydrogel with and without AgNPs in each well, and the clear colony counting of the samples was measured.

2.8 | Animal study

The efficacy of the produced hydrogel dressings on the excisional wound healing of full-thickness wounds in rats was studied in this study. The 12 young Sprague-Dawley male rats (200 g) were divided into three groups: control, HMC-HA hydrogels, and HMC-HA/AgNPs hydrogels. Each group was kept in its cage and supplied normal rodent feed and water ad libitum at a temperature of 25°C under sanitary circumstances. For each rat in the cleaned area, a surgical blade was used to create a wound with a surface area of 1.5×1.5 cm^2. The animals were anesthetised with a 20 mg kg^{-1} intraperitoneal injection of ketamine-xylazine combination. The rats were then returned to the animal laboratory and placed under typical water, food, and lighting conditions. All animal procedures were authorised by the Animal Research Committees of Chengyang District People's Hospital during all phases of the investigation. Following that, the pastes of the aforementioned four freshly made dressings were utilised to tightly cover the wound surface, with PBS being used for the control group rats. At predetermined time intervals, the wound area was measured. After 2, 4, 8, and 16 days, the wound healing impact was observed and analysed.

2.9 | Histological analysis

Wounded skin tissue samples were processed using normal histological procedures at the end of the experiment, and microscopic changes in skin were noted. CO_2 gas asphyxiation was used to kill the rats on days 2, 4, 8, and

16. Each rat's wound tissue was taken separately for histological analysis. The wound samples were first treated in 4% paraformaldehyde for a week after being taken. The HMC-HA and HMC-HA/AgNPs hydrogels were next dehydrated and embedded in paraffin wax. All animals' tissue histology was compared with that of the control and reference standard animals using an Olympus BX 60 microscope at magnifications of 4× for hematoxylin and eosin-stained tissue and 40× for Masson's trichrome staining.

2.10 | Statistical analysis

Experimental data from the studies were analysed using Student's t test. Results were analysed by triplicate and the results are reported as mean ± SD. The statistical significance of the data was as $P < .05$.

3 | RESULTS AND DISCUSSIONS

3.1 | Mechanism of hydrogel formation and optical properties

As a result, intra-molecular and inter-molecular chain hydrophobic contacts emerge, culminating in gelation as the number of interactions grows, thus forming a broad "hydrophobicity cross-linked" network. The hydrogen interactions induced by the functional carboxyl and hydroxyl groups, as well as the participation of —NH and —COO— ionisable groups, all contribute to the production of HMC-HA hydrogel (Figure 1A). AgNO$_3$ was added to the HMC-HA hydrogel after processing, resulting in surface plasmon resonance (SPR), which indicated AgNPs fabrication in good agreement with UV-visible spectra. On organic molecules, Ag$^+$ has a severe oxidising action. The presence of carboxyl and hydroxyl groups in the polymeric units of the HMC-HA hydrogel

enhances Ag$^+$ chelate formation.[23] Figure 1B depicts the UV absorption spectrum. Silver nitrate (AgNO$_3$) is decomposed into silver (Ag$^+$) and nitrate (NO$_3^-$) ions in an aqueous solution. The peak at 420 nm indicates that AgNPs were successfully synthesised, while the peak at 382 nm indicates that AgNPs were modified using HMC-HA hydrogel.[24] The SPR band evolves as a function of Ag$^+$ concentration, the specific absorption peak derived from the SPR of AgNPs should be positioned between 400 and 450 nm, according to the literature research.[25] The successful synthesis of AgNPs in situ was validated by an increase in the absorbance of the HMC-HA hydrogels solution at 420 nm, as well as an increase in the AgNPs concentration solution.[26] The development of fewer NPs and more aggregates was suggested by the rise in absorbance for the one created at 2.0% Ag$^+$ concentration. This result showed that the AgNPs loaded in the HMC-HA hydrogel composite had a stable behaviour.

## 3.2 | SEM and TEM analysis of HMC-HA/AgNPs

SEM and TEM analyses were used to examine the surface morphology of the HMC-HA hydrogel containing AgNPs, as illustrated in Figures 2-4. HMC-HA hydrogel has a honeycomb-like three-dimensional porous structure, as seen in Figure 2. The honeycomb structure and cross-linking of the HMC-HA hydrogels were visible in SEM pictures.[27] The dried HMC-HA hydrogels had a cross-linked network and a porous surface, which aids in the long-term release of extract and AgNPs.[28] The porous structure of hydrogels was maintained after the insertion of AgNPs incorporating HMC-HA hydrogel, but the pore size was dependent on the concentration of AgNPs (Figure 2B-D): the higher the content, the smaller the pore size.[29] The physical interaction (ie, hydrogen bonds) among the functional groups of the blended component was demonstrated by the homogeneity of the cross-linked
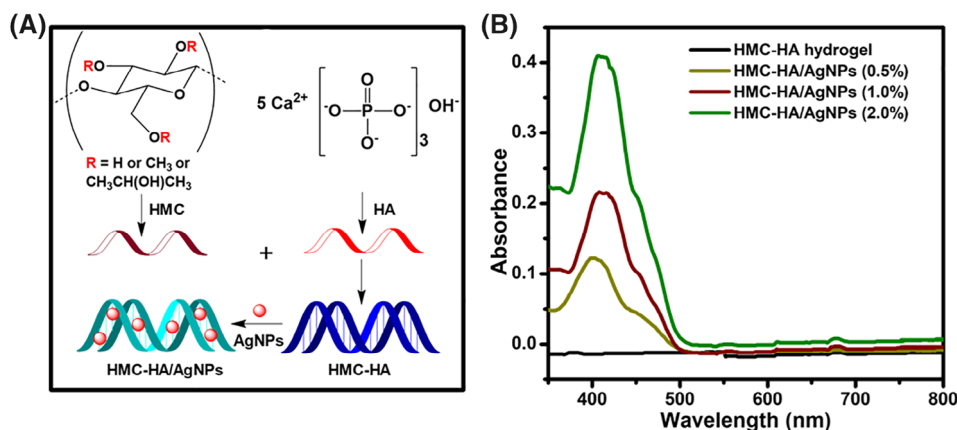

FIGURE 1 A, The schematic representation of HMC-HA hydrogel containing AgNPs and B, UV-Vis absorption spectra of HMC-HA hydrogels containing AgNPs at different concentrations (0.5, 1.0, and 2.0% wt/wt)

FIGURE 2   SEM images of HMC-HA hydrogel, A, and HMC-HA hydrogel containing AgNPs, B, 0.5%, C, 1.0%, and D, 2.0%
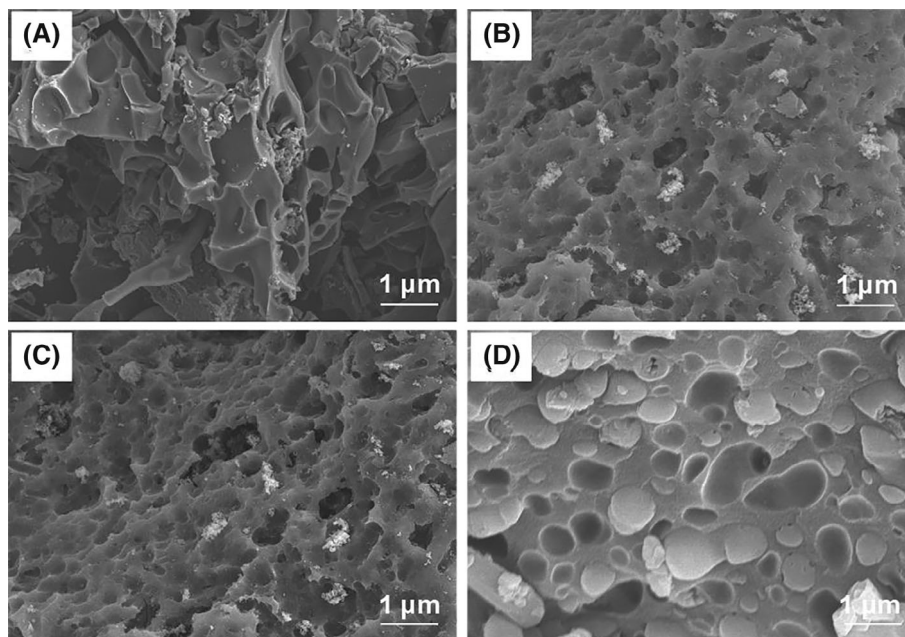
FIGURE 3   SEM pore size histogram image of HMC-HA hydrogel, A, and HMC-HA hydrogel containing AgNPs, B, 0.5%, C, 1.0%, and D, 2.0%
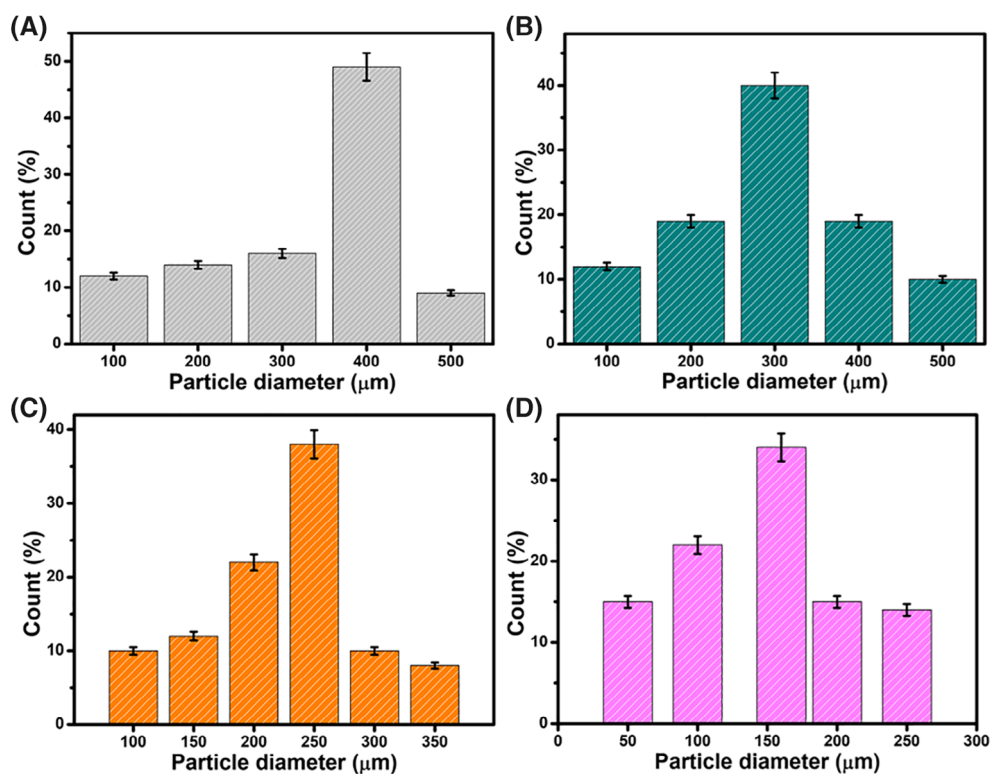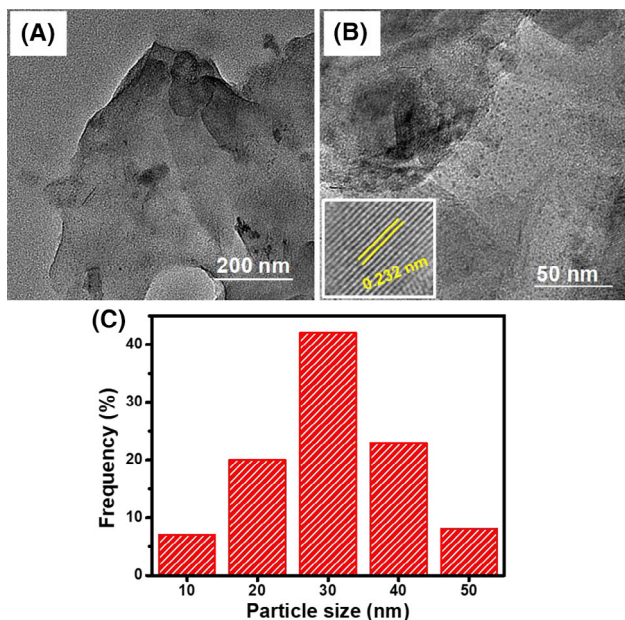
network of HMC-HA hydrogels. The pore size of HMC-HA hydrogels appears to decrease with the addition of AgNPs, as shown in Figure 3A-D. The network space was filled with AgNPs, and the interaction between AgNPs and HMC-HA caused the hydrogel space to be compressed, which caused this result. When the surface morphology of spherical HMC-HA and HMC-HA/AgNPs hydrogels was examined at a greater resolution, the surface morphology showed a highly interconnected porous structure with an average pore size of 500 to 50 μm.[30] The porous structure of the material aids in the absorption of huge volumes of wound exudates from the wound surface. A cross-linked network with optimal porosity promotes increased cellular penetration and nutritional activities while offering ample surface and strength for cellular operation. The amorphous nature of HMC-HA hydrogel confirmed by transmission electron morphology is shown in Figure 4A. The representative TEM image in

Figure 4B shows that the HMC-HA hydrogels containing AgNPs exhibit a spherical shape with an average diameter of 30 nm (Figure 4C).[31] The uniform distribution of the AgNPs was confirmed in HRTEM analysis indicating that the AgNPs were well stabilised by the HMC-HA
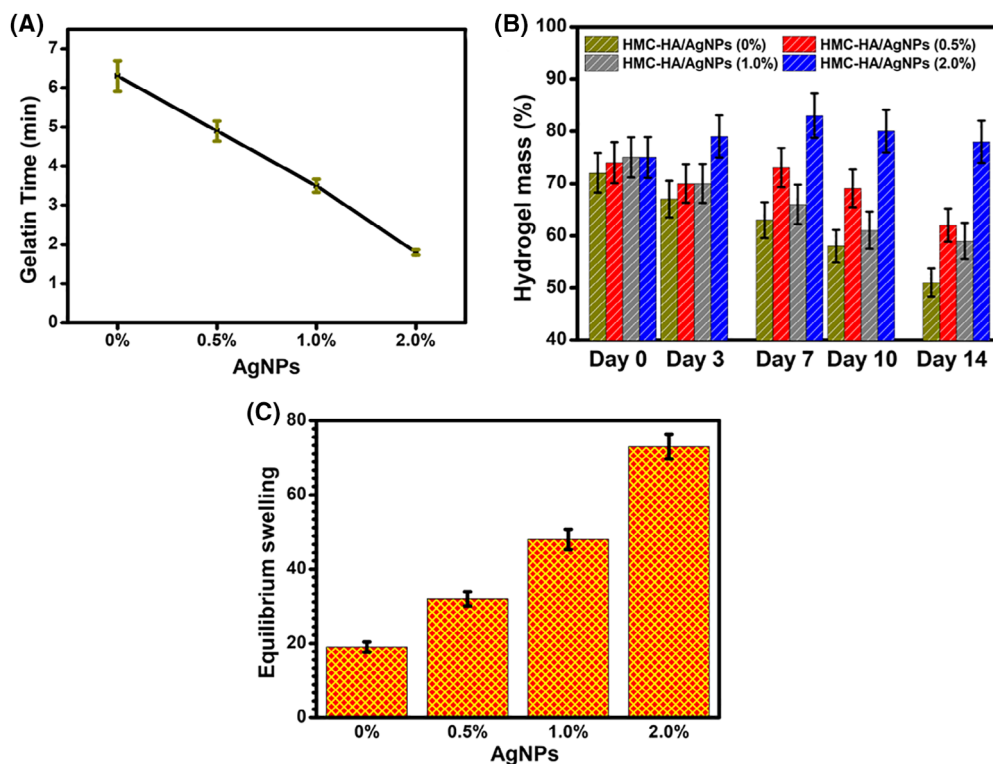
hydrogel. HRTEM examinations of the AgNPs including HMC-HA hydrogel showed the long-range atomic structure through the lattice fringes of atoms, demonstrating the AgNPs' great crystallinity (inset Figure 4B).[32] The particle size obtained by TEM was very close to the crystalline size, and XRD analytical data corroborated this.

3.3 | Gelation time, in vitro degradation, and equilibrium swelling of hydrogels

The gelation time was investigated by varying the AgNPs concentration (0.5, 1.0, and 2.0% wt/wt) with a fixed HMC-HA (50 mg/mL) hydrogels. As shown in Figure 5A, the gelation time decreased from 6.3 to 1.8 minutes upon increasing the AgNPs concentrations (2.0% wt/wt) at 37°C. The gelation time for HMC-HA hydrogels was found to be longer than that for AgNPs directly grafted with methoxyl or hydroxyl groups.[33] The gelation rate of HMC-HA/AgNPs-2.0% hydrogel was the fastest, which exhibited a substantially higher gelation rate than HMC-HA/AgNPs-1.0% and HMC-HA/AgNPs-0.5% ($P < .05$). On the other hand, a more cationic group of HA could increase the hydrophilicity of HMC-HA hydrogels, which prolonged the time of gelation caused by the hydrophobic interaction between HMC-HA hydrogels and AgNPs.[34] Figure 5B shows the in vitro degradation of AgNPs and HMC-HA hydrogels, respectively, carried out by incubating in PBS at 37°C. A rise in cross-linking density leads

FIGURE 4 TEM images of HMC-HA hydrogel, A, HMC-HA hydrogel containing AgNPs, B, with inset figure; HRTEM lattice fringe of AgNPs, and histogram image of the average sizes of HMC-HA hydrogel containing AgNPs, C

FIGURE 5 A, Gelation time; B, in vitro degradation; and C, Swelling ratio of HMC-HA hydrogels as a function of AgNPs concentration

to a decrease in water content and a loss of mass weight. The complete degradation of HMC-HA hydrogels in 2.0% of AgNPs concentration was after 14 days.[35] The weight remaining ratios of AgNPs in the MC-HA hydrogels at day 14 were $51.3 \pm 2.1\%$, $62.6 \pm 1.3\%$, $59.8 \pm 0.9\%$, and $78.3 \pm 1.9\%$, respectively. It was discovered that increasing the AgNPs content in HMC-HA hydrogels causes increased swelling and the creation of a loose network, which increases the percentage degradation. The results can be explained by the fact that at greater AgNPs concentrations, the HMC-HA hydrogels cleave faster. The improved degradation rate of the sample with AgNPs could be explained by morphological properties such as the porous gel structure of HMC-HA hydrogels.[36] The swelling ratio was used to assess the ability of biomaterials to absorb and retain water, as well as their stability. Figure 5C shows the swelling ratios calculated for several samples with varying amounts of AgNPs inserted into HMC-HA hydrogels vs immersion time. The swelling of hydrogels is well known to be substantially influenced by the functional groups connected to them. Both HMC and HA feature a significant number of hydrophilic groups that can easily hydrate with water, such as $-OCH_3$, $-NH$, and $-OH$. As the AgNPs concentration increased from 0.5 to 2.0% ($P < .05$), the swelling value increased significantly (Figure 5C). The trend of the swelling ratio as Ag^+ concentration changes corresponds to the mechanical strength and AgNPs absorption of HMC-HA hydrogels.[37] As a result, formulations based on HMC-HA hydrogels containing 2.0% wt. AgNPs were considered for further research.

3.4 | Surface analysis of HMC-HA/AgNPs

The FT-IR was also used to characterise the HMC-HA-hydrogel, AgNPs, and HMC-HA hydrogel containing AgNPs (Figure 6A). The pure HMC showed the characteristic peaks at 3451 cm^{-1} ($-OH$), 2897 and 2834 cm^{-1} (C—H), 1642 cm^{-1} (C=O), 1454 and 1372 cm^{-1} ($-OCH_3$ and $-CH_3$ groups), 1194 and 1051 cm^{-1} ($-C-O$) and 945 cm^{-1} (C—C) of the glucopyranose ring of HMC functional groups.[16] The FT-IR spectra of the HMC-HA hydrogel are shown in Figure 6A, with multiple distinct peaks indicating its growth. The intensity vibration between 3126, 3429, and 3512 cm^{-1} produces a satisfactory signal, which could be attributed to the HMC alcohol and the hydrogels' hydration grade. In the spectra of HMC-HA/AgNPs, the usual peaks of C=C stretching vibration of the aromatic ring (1617 cm^{-1}) formed from HMC-HA hydrogel can be seen. The C—O stretching of phenolic acid is allocated to the band at 1058 cm^{-1}, while the O—H functional groups from carboxyl or phenols are assigned to the band at 3446 cm^{-1}. AgNPs had distinct peaks in the FT-IR spectrum at 1538, 1651, 1228, 2919, 2849, and 3288 cm^{-1}.[38] The vibrational characteristic peak of AgNPs was found in the 400 to 1000 cm^{-1} range. Because of the stretching vibration of Ag^+ in AgNPs, the peak appeared at 500 cm^{-1}. All of the typical peaks of HMC, HA, and AgNPs were observed when comparing the spectral characteristics of HMC-HA/AgNPs to the HMC-HA hydrogel, with peaks displaced to 3654, 3574, 2812, 1653, 1545, 1408, 1142, 935, 855, 681, and 541 cm^{-1}. The carbonyl, alkyl, and hydroxyl groups in the HMC-HA hydrogel have a higher affinity for interacting with metal ions, promoting silver ion reduction into AgNPs, according to these findings. These findings show that AgNPs can be successfully modified using the HMC-HA hydrogel. Figure 6B shows the XRD patterns of HMC-HA hydrogel, AgNPs, and HMC-HA/AgNPs. In general, XRD analysis showed whether the materials were crystalline or amorphous. The semi-amorphous character of the HMC-HA hydrogel was shown by a typical diffraction peak at $2\theta = 26.54°$ (Figure 6B).[39] The synthesised AgNPs had a strong intensity peaks plane, which corresponded to (111), (200), (220), and (311) considerations of face-centred cubic structure metallic silver, and agreed with JCPDS File No: 04-0783, showing the crystalline nature of the AgNPs.[40] The
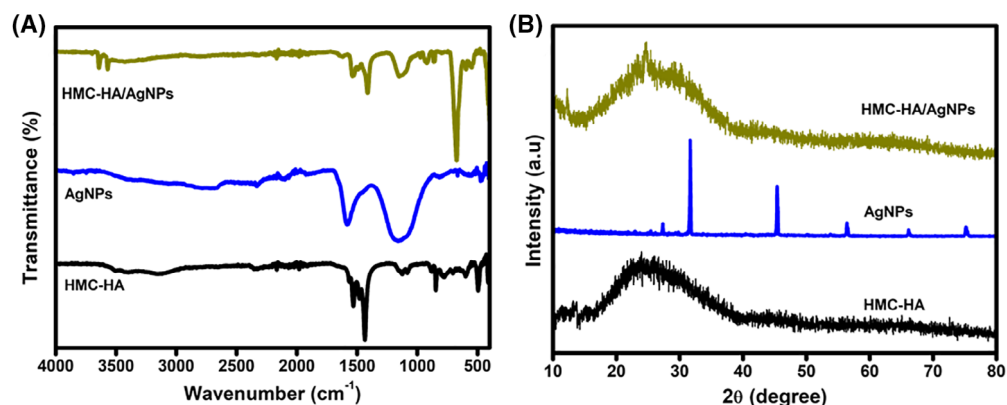

FIGURE 6 A, Fourier transform infrared spectrum (FT-IR) spectra and B, XRD patterns of the HMC-HA hydrogel, AgNPs, and HMC-HA/ AgNPs hydrogel

face-centred cubic structure of AgNPs was confirmed by substantial diffraction subsequent peaks in HMC-HA/AgNPs at $2\theta = 24.32°$, $28.37°$, and $42.04°$. AgNPs on the HMC-HA hydrogel has been efficiently integrated as a result of the lowered intensity peaks. The Debye-Scherrer equation was used to compute the particle size of the AgNPs, which was found to be around 28 nm,[41] which was consistent with the TEM observations.

3.5 | Antibacterial activity of the MC-HA/AgNPs

Colony counting was used to measure the antibacterial activity of HMC-HA and HMC-HA/AgNPs hydrogels (Table 1). As model organisms, Gram-negative *E coli* and Gram-positive *S aureus* were chosen. As a comparison, the control group and the HMC-HA hydrogel were used. The colony formed in the HMC-HA hydrogel matrix, and the maximum rate of bacterial death was recorded in 78.9 ± 2.61% of the cases.[42] The HMC-HA/AgNPs hydrogel treatment had a strong antibacterial impact, which was mostly because of the long time necessary for Ag^+ sterilisation and the adequate release of Ag^+ from the hydrogel throughout the incubation period.[43] It is also worth noting that silver ions antibacterial properties are thought to be because of its role as a contact active substance or silver ion released. Surprisingly, the HMC-HA hydrogel treatment group declined dramatically ($P < .05$) in the presence of AgNPs, and more than 95.6 ± 1.93% of the bacteria were destroyed. This action could have been triggered by higher surface correlations between HMC-HA/AgNPs and bacteria. In comparison to *E coli*, HMC-HA/AgNPs had the highest antibacterial activity than *S aureus*, according to the data.[44] In *E coli*, this could be because of the influence of a double membrane. The antibacterial action of silver ions loaded HMC-HA hydrogel hydrogels could be related to the fact that AgNPs can interact with phosphorus-containing proteins from cells, targeting the respiratory chain and ultimately leading to cell death through cell division.[45] The synergistic effect of the remarkable photothermal effect of HMC-HA/AgNPs

hydrogel and the innate antibacterial property of Ag^+ were primarily responsible for the good antibacterial effect.

3.6 | In vivo wound healing effect

The wound area was measured when being harvested for macroscopic analysis of the excisional wound healing process, taking into account the type of hydrogel utilised and the period of wound removal.[46] The ability of this synergetic antibacterial method to cure wounds in mice infected with bacteria was also tested in vivo. The animal models were Sprague-Dawley male rats with *S aureus*-infected lesions on their backs. First, digital photographs of each sample were obtained at predetermined intervals (Figure 7A). Every 2 days, representative photographs of wound closure from various treatment groups were taken, and the therapeutic effect and potential adverse effects were calculated. On the other hand, after 16 days, the wound treated with HMC-HA/AgNPs hydrogel generated new skin and demonstrated almost complete recovery.[35] The rate of wound contraction in all experimental groups is depicted in Figure 7B. When the wound healing potential of control, HMC-HA hydrogel, and HMC-HA hydrogel-loaded AgNPs was evaluated, it was discovered that only 2 days after initial wound treatment, the AgNPs impregnated HMC-HA hydrogel group had 39.1 ± 2.4% wound area contraction, compared with 28.6 ± 1.3% in the control group and 16.3 ± 0.6% in the HMC-HA hydrogel-loaded AgNPs groups. The effective activity of the HMC-HA hydrogel with the inclusion of AgNPs in the community reacting to HMC was seen on the 2, 4, and 8 postoperative days. The HMC-HA/AgNPs dressing group had a wound healing rate of 94.5 ± 1.4%, which was higher than the HMC-HA hydrogel (56.3%) and control (36.2 ± 0.8%) groups, implying that the synergistic impact ($P < .05$) contributed to its improved healing capability.[11,47-49] The growth of granulation tissue after 16 days can be attributed to the effective behaviour of the HMC-HA/AgNPs hydrogel. The wound healing rate for the HMC-HA/AgNPs hydrogel treatment group was

TABLE 1 The bacterial reduction rate of control, HMC-HA hydrogel, and HMC-HA/AgNPs hydrogels

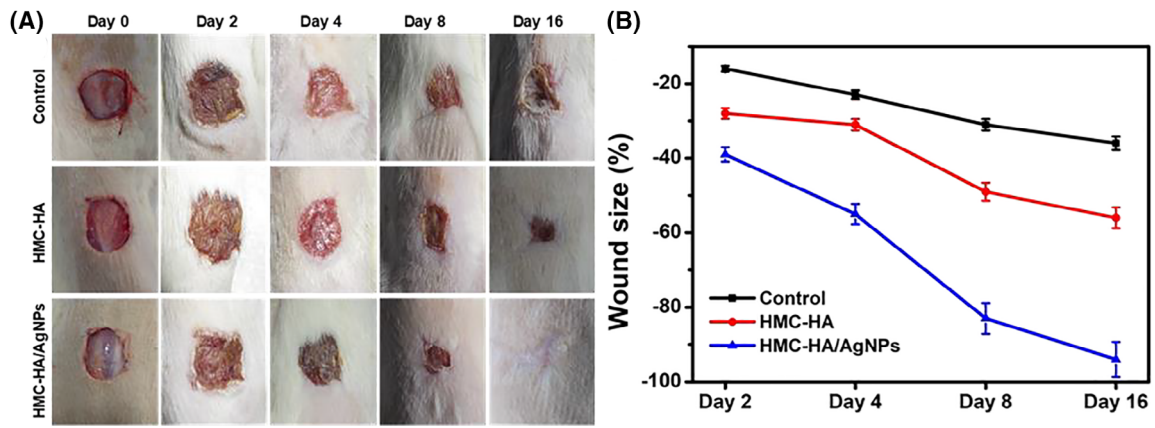|	*Staphylococcus aureus*		*Escherichia coli*	
	No. of bacterial at 24 hours	Bacterial reduction rate (%)	No. of bacterial after 24 hours	Bacterial reduction rate (%)
Control	2.0×10^5	-	2.0×10^5	-
MC-HA	<52	74.3 ± 0.41	<52	78.9 ± 2.61
MC-HA/ AgNPs	<55	92.8 ± 1.32	<55	95.6 ± 1.93

FIGURE 7 A, In vivo study of control, HMC-HA, and HMC-HA/AgNPs as a wound dressing and B, the evaluation of wound reduction rate (%)
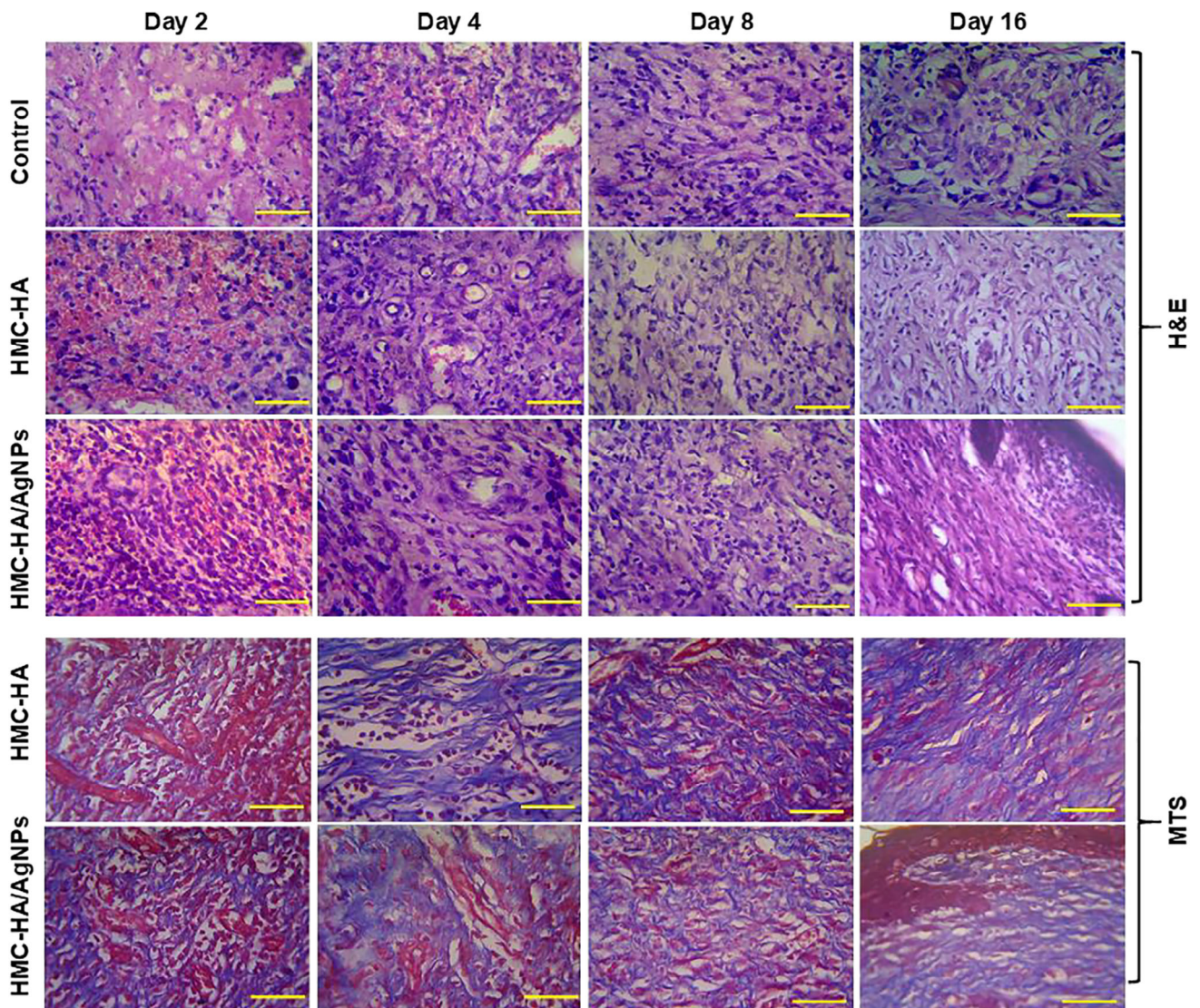

FIGURE 8 Hematoxylin and eosin (H&E)-stained and MTS-stained sections of the granulation tissue of control, HMC-HA, and HMC-HA/AgNPs on a postoperative day 2, 4, 8, and 16 (scale bar ∼100 μm)

substantially faster than the wound healing rate for the HMC-HA wound dressing treatment group, as shown in Figure 7, showing that the HMC-HA/AgNPs hydrogel has superior antibacterial and wound healing properties. Images captured with a camera, as shown in Figure 7A, corroborate these findings.

3.7 | Histological investigations

On days 2, 4, 8, and 16, histological examinations of hematoxylin and eosin (H&E) and Masson's trichrome stained wound tissue were made to establish collagen deposition and skin regeneration (Figure 8). On days 2 to 16, the number of blood vessels and reepithelialisation in the control and HMC-HA hydrogel groups were low compared with the other hydrogel groups. On days 2 and 4, blood mixed HMC-HA/AgNPs hydrogel treated skin showed significant neovascularization and fibroblast infiltration,[50] as well as partial dermal layer formation with collagen bundles on day 8.[51] The epithelial tissue was not entirely produced in the control and HMC-HA hydrogel wounds after 16 days, and mature blood vessels and inflammatory cells were fairly evident. The dermal layer of wounded skin was entirely covered with an epithelial layer in the samples treated with the HMC-HA/AgNPs hydrogel at day 16 post-surgery.[52] In addition, the dermis had a large number of fibroblasts and even inflammatory cells. The most striking trait that distinguished AgNPs composite gel from commercial formulations was the presence of a larger number of undamaged cells in the dermis, which means fewer scars.[53] The AgNPs group showed strong dermal layer development and a high rate of maturation of proliferating cell bodies.[54] As a result, the findings backed up our hypothesis and provided evidence for the synergistic potential of HMC-HA hydrogel with AgNPs treatment to speed wound healing in diabetes-induced animal models.

4 | CONCLUSION

In conclusion, HMC and HA-based hydrogels with only 2 wt% 0.5 wt% polymers appear to have a very porous morphology when compared with chemically cross-linked HMC-HA hydrogels. When 2.0 wt% AgNPs are added to an HMC-HA hydrogel matrix, the latter cross-links with the former, resulting in an HMC-HA hydrogel matrix with improved optical, spectral, and morphological properties, which can be used as an effective antibacterial and wound healing process in the nursing care of burn injury in children. The Debye-Scherrer equation was used to compute the particle size of the AgNPs,

which was found to be around 28 nm, which was consistent with the TEM observations. The inclusion of AgNPs demonstrated outstanding stability on the gelation duration, in vitro degradation, and swelling properties because of the probable inter-chain cross-linking of HMC-HA hydrogel. Antimicrobial investigations using HMC-HA and HMC-HA hydrogels loaded with AgNPs show good resistance against Gram-positive and Gram-negative bacteria, with *E coli* and *S aureus* showing superior colony formation suppression. In an in vivo full-thickness excisional wound healing mouse model, the proposed composite HMC-HA hydrogels loaded AgNPs dressing significantly improved wound closure by day 16, and histological examination of the tissue in the wounded area showed rapid reepithelialisation, differentiated dermis, and epidermis, with minimal scar tissues. These findings support the potential of HMC-HA hydrogels loaded with AgNPs for wound healing and burn injury nursing care in children.

CONFLICT OF INTEREST
The authors declare no conflicts about this research investigation.

DATA AVAILABILITY STATEMENT
Research data are not shared.

ORCID
Jianye Jiang https://orcid.org/0000-0001-7636-7237

REFERENCES
1. Sen CK. Human wounds and its burden: an updated compendium of estimates. *Adv Wound Care*. 2019;8(2):39-48.
2. Sen CK, Gordillo GM, Roy S, et al. Human skin wounds: a major and snowballing threat to public health and the economy. *Wound Repair Regen*. 2009;17(6):763-771.
3. Frykberg RG, Banks J. Challenges in the treatment of chronic wounds. *Adv Wound Care*. 2015;4(9):560-582.
4. Naskar A, Kim KS. Recent advances in nanomaterial-based wound-healing therapeutics. *Pharmaceutics*. 2020;12(6): 499 (1-20).
5. Kadiyala U, Kotov NA, VanEpps JS. Antibacterial metal oxide nanoparticles: challenges in interpreting the literature. *Curr Pharm Des*. 2018;24(8):896-903.
6. Mikhailova EO. Silver nanoparticles: mechanism of action and probable bio-application. *J Funct Biomater*. 2020;11(4): 84 (1-26).
7. Choudhury H, Pandey M, Lim YQ, et al. Silver nanoparticles: Advanced and promising technology in diabetic wound therapy. *Mater Sci Eng C*. 2020;11:110925.
8. Kalantari K, Mostafavi E, Afifi AM, et al. Wound dressings functionalized with silver nanoparticles: promises and pitfalls. *Nanoscale*. 2020;12(4):2268-2291.
9. Yun'an Qing LC, Li R, Liu G, et al. Potential antibacterial mechanism of silver nanoparticles and the optimization of

orthopedic implants by advanced modification technologies. *Int J Nanomedicine*. 2018;13:3311-3327.

10. Salleh A, Naomi R, Utami ND, et al. The potential of silver nanoparticles for antiviral and antibacterial applications: a mechanism of action. *Nanomaterials*. 2020;10(8):1566 (1-20).

11. Krishnan PD, Banas D, Durai RD, et al. Silver nanomaterials for wound dressing applications. *Pharmaceutics*. 2020;12(9):821 (1-24).

12. Alven S, Aderibigbe BA. Chitosan and cellulose-based hydrogels for wound management. *Int J Mol Sci*. 2020;21(24):9656 (1-30).

13. Zhu J, Marchant RE. Design properties of hydrogel tissue-engineering scaffolds. *Expert Rev Med Devices*. 2011;8(5):607-626.

14. Shaghaleh H, Xu X, Wang S. Current progress in production of biopolymeric materials based on cellulose, cellulose nanofibers, and cellulose derivatives. *RSC Adv*. 2018;8(2):825-842.

15. Portela R, Leal CR, Almeida PL, Sobral RG. Bacterial cellulose: a versatile biopolymer for wound dressing applications. *J Microbial Biotechnol*. 2019;12(4):586-610.

16. Bashir S, Zafar N, Lebaz N, Mahmood A, Elaissari A. Hydroxypropyl methylcellulose-based hydrogel copolymeric for controlled delivery of galantamine hydrobromide in dementia. *Processes*. 2020;8(11):1350 (1-21).

17. Joshi SC. Sol-gel behavior of hydroxypropyl methylcellulose (HPMC) in ionic media including drug release. *Materials*. 2011;4(10):1861-1905.

18. Ghosal K, Chakrabarty S, Nanda A. Hydroxypropyl methylcellulose in drug delivery. *Der Pharma Sin*. 2011;2(2):152-168.

19. Kattimani VS, Kondaka S, Lingamaneni KP. Hydroxyapatite—past, present, and future in bone regeneration. *Bone Tissue Regen Insights*. 2016;7:9-19.

20. Roohani-Esfahani SI, Nouri-Khorasani S, Lu Z, Appleyard R, Zreiqat H. The influence hydroxyapatite nanoparticle shape and size on the properties of biphasic calcium phosphate scaffolds coated with hydroxyapatite–PCL composites. *Biomaterials*. 2010;31(21):5498-5509.

21. Dong C, Zhang X, Cai H. Green synthesis of monodisperse silver nanoparticles using hydroxy propyl methyl cellulose. *J Alloys Compd*. 2014;583:267-271.

22. George J, Kumar R, Sajeevkumar VA, et al. Hybrid HPMC nanocomposites containing bacterial cellulose nanocrystals and silver nanoparticles. *Carbohydr Polym*. 2014;105:285-292.

23. Shen X, Shamshina JL, Berton P, Gurau G, Rogers RD. Hydrogels based on cellulose and chitin: fabrication, properties, and applications. *Green Chem*. 2016;18(1):53-75.

24. Ashraf JM, Ansari MA, Khan HM, Alzohairy MA, Choi I. Green synthesis of silver nanoparticles and characterization of their inhibitory effects on AGEs formation using biophysical techniques. *Sci Rep*. 2016;6(1):20414.

25. Mukherji S, Bharti S, Shukla G, Mukherji S. Synthesis and characterization of size-and shape-controlled silver nanoparticles. *Phys Sci Rev*. 2018;4:20170082.

26. Kondeti VS, Gangal U, Yatom S, Bruggeman PJ. Ag+ reduction and silver nanoparticle synthesis at the plasma–liquid interface by an RF driven atmospheric pressure plasma jet: mechanisms and the effect of surfactant. *J Vac Sci Technol A*. 2017;35(6):061302.

27. Xia LW, Xie R, Ju XJ, Wang W, Chen Q, Chu LY. Nano-structured smart hydrogels with rapid response and high elasticity. *Nat Commun*. 2013;4(1):2226.

28. Wang T, Zhang F, Zhao R, et al. Polyvinyl Alcohol/Sodium alginate hydrogels incorporated with silver nanoclusters via green tea extract for antibacterial applications. *Des Monomers Polym*. 2020;23(1):118-133.

29. Kazeminava F, Arsalani N, Ahmadi R, Kafil HS, Geckeler KE. A facile approach to incorporate silver nanoparticles into solvent-free synthesized PEG-based hydrogels for antibacterial and catalytical applications. *Polymer Test*. 2020;10:106909.

30. Annabi N, Nichol JW, Zhong X, et al. Controlling the porosity and microarchitecture of hydrogels for tissue engineering. *Tissue Eng Part B Rev*. 2010;16(4):371-383.

31. Yunusov KE, Sarymsakov AA, Jalilov JZ, Atakhanov AA. Physicochemical properties and antimicrobial activity of nanocomposite films based on carboxymethylcellulose and silver nanoparticles. *Polym Adv Technol*. 2021;32(4):1822-1830.

32. Yu Z, Hu C, Guan L, Zhang W, Gu J. Green synthesis of cellulose nanofibrils decorated with Ag nanoparticles and their application in colorimetric detection of L-cysteine. *ACS Sustain Chem Eng*. 2020;8(33):12713-12721.

33. Lustosa AK, de Jesus Oliveira AC, Quelemes PV, et al. In situ synthesis of silver nanoparticles in a hydrogel of carboxymethyl cellulose with phthalated-cashew gum as a promising antibacterial and healing agent. *Int J Mol Sci*. 2017;18(11):2399 (1-15).

34. Das SK, Parandhaman T, Dey MD. Biomolecule-assisted synthesis of biomimetic nanocomposite hydrogel for hemostatic and wound healing applications. *Green Chem*. 2021;23(2):629-669.

35. Diniz FR, Maia RC, Rannier L, et al. Silver nanoparticles-composing alginate/gelatine hydrogel improves wound healing in vivo. *Nanomaterials*. 2020;10(2):390 (1-16).

36. Rodríguez Nuñez YA, Castro RI, Arenas FA, et al. Preparation of hydrogel/silver nanohybrids mediated by tunable-size silver nanoparticles for potential antibacterial applications. *Polymers*. 2019;11(4):716 (1-13).

37. Helmiyati NG, Abbas GH, Budianto E. Nanocomposite hydrogel-based biopolymer modified with silver nanoparticles as an antibacterial material for wound treatment. *J Appl Pharma Sci*. 2019;9(11):1-9.

38. Jyoti K, Baunthiyal M, Singh A. Characterization of silver nanoparticles synthesized using *Urtica dioica* Linn. leaves and their synergistic effects with antibiotics. *J Radiat Res Appl Sci*. 2016;9(3):217-227.

39. Baron RI, Biliuta G, Socoliuc V, Coseri S. Affordable magnetic hydrogels prepared from biocompatible and biodegradable sources. *Polymers*. 2021;13(11):1693 (1-15).

40. Vanaja M, Annadurai G. Coleus aromaticus leaf extract mediated synthesis of silver nanoparticles and its bactericidal activity. *Appl Nanosci*. 2013;3(3):217-223.

41. Tag HM, Saddiq AA, Alkinani M, Hagagy N. Biosynthesis of silver nanoparticles using Haloferax sp. NRS1: image analysis, characterization, in vitro thrombolysis and cytotoxicity. *AMB Expr*. 2021;11(1):75 (1-12).

42. Li S, Dong S, Xu W, et al. Antibacterial hydrogels. *Adv Sci*. 2018;5(5):1700527 (1-17).

43. Alcântara MT, Lincopan N, Santos PM, et al. Simultaneous hydrogel crosslinking and silver nanoparticle formation by using ionizing radiation to obtain antimicrobial hydrogels. *Radiat Phys Chem*. 2020;169:108777.

44. Galdiero S, Falanga A, Vitiello M, Cantisani M, Marra V, Galdiero M. Silver nanoparticles as potential antiviral agents. *Molecules*. 2011;16(10):8894-8918.

45. Allawadhi P, Singh V, Khurana A, et al. Silver nanoparticle based multifunctional approach for combating COVID-19. *Sens Int*. 2021;2:100101.

46. Yao Y, Zhang A, Yuan C, Chen X, Liu Y. Recent trends on burn wound care: hydrogel dressings and scaffolds. *Biomater Sci*. 2021;9:4523-4540. https://doi.org/10.1039/D1BM00411E

47. Paladini F, Pollini M. Antimicrobial silver nanoparticles for wound healing application: progress and future trends. *Materials*. 2019;12(16):2540 (1-16).

48. Pangli H, Vatanpour S, Hortamani S, Jalili R, Ghahary A. Incorporation of silver nanoparticles in hydrogel matrices for controlling wound infection. *J Burn Care Res*. 2020;41:1-9.

49. Masood N, Ahmed R, Tariq M, et al. Silver nanoparticle impregnated chitosan-PEG hydrogel enhances wound healing in diabetes induced rabbits. *Int J Pharm*. 2019;559:23-36.

50. Li R, Xu Z, Jiang Q, Zheng Y, Chen Z, Chen X. Characterization and biological evaluation of a novel silver nanoparticle-loaded collagen-chitosan dressing. *Regen Biomater*. 2020;7(4): 371-380.

51. Singla R, Soni S, Patial V, et al. Cytocompatible anti-microbial dressings of syzygium cumini cellulose nanocrystals decorated with silver nanoparticles accelerate acute and diabetic wound healing. *Sci Rep*. 2017;7(1):10457 (1-13).

52. Mihai MM, Dima MB, Dima B, Holban AM. Nanomaterials for wound healing and infection control. *Materials*. 2019;12(13): 2176 (1-16).

53. Azharuddin M, Zhu GH, Das D, et al. A repertoire of biomedical applications of noble metal nanoparticles. *Chem Commun*. 2019;55(49):6964-6996.

54. Sarhan OM, Hussein RM. Effects of intraperitoneally injected silver nanoparticles on histological structures and blood parameters in the albino rat. *Int J Nanomedicine*. 2014; 9:1505-1517.